Electronic Supplementary Material (ESI) for Environmental Science: Processes & Impacts.

Evidence for non-electrostatic interactions between a pyrophosphate-functionalized uranyl peroxide nanocluster and iron (hydr)oxide minerals

Luke R. Sadergaski, Samuel N. Perry, Luke R. Tholen, and Amy E. Hixon*

Department of Civil & Environmental Engineering & Earth Sciences, University of Notre Dame,
Notre Dame, IN 46556 USA

*Corresponding author. Phone: +1 574 631 1872; Fax: +1 574 631 9236; E-mail: ahixon@nd.edu

Electronic Supplementary Information:

Extended Experimental

Figures

Tables

Extended Experimental

Electrospray ionization mass spectrometry

Electrospray ionization mass spectrometry (ESI-MS) has been used successfully as a method for "fingerprinting" nanoclusters in solution.[1] In this study, ESI-MS was used to confirm that the $U_{24}Pp_{12}$ stock solution was monodisperse. ESI-MS was also used to characterize the persistence of $U_{24}Pp_{12}$ after being in contact with goethite and hematite by measuring the resulting supernatant at various points throughout the batch sorption experiments. Spectra were collected in negative ion mode using a Bruker microTOF-Q II high resolution quadrupole time-of-flight spectrometer. Samples were introduced by direct infusion rates between 350 – 450 µL min^{-1} and data were averaged over 120 seconds from 500 – 5000 m/z.

ESI-MS results demonstrated that the $U_{24}Pp_{12}$ clusters remained intact in solutions containing goethite and hematite for the duration of the batch sorption experiments. The average molecular weight of multiple charge states determined by ESI-MS remained constant throughout the sorption experiments at pH 9 (see Fig. S23).

X-ray photoelectron spectroscopy

X-ray photoelectron spectroscopy (XPS) was used measure the photoelectron spectrum of uranium to determine the valence state of uranium. Spectra were collected using a PHI VersaProbe II X-ray photoelectron spectrometer with monochromatic Al K radiation using a pass energy of 29.35 eV and a 100-µm spot size. $U_{24}Pp_{12}$ crystals and reacted mineral samples were placed on double-stick tape for analysis. Surface neutralization was performed automatically and the measured U 4*f*, P 2*p*, Na 1*s*, and Li 1*s* binding energies were referenced by fixing the position of the C 1*s* peak to 285.0 eV. Shirley background and asymmetric peak shape profile parameters were used to model fitted U $4f_{5/2}$ peaks.[2,3] Gaussian-Lorentzien peak shaper parameters were used to model fitted Fe 2*p*, P 2*p*, Na 1*s*, O 1*s* and Li 1*s* lines.[4,5]

SEM-EDS analysis

Scanning electron microscopy (SEM) images were taken with a JEOL JCM-6000 Plus Neoscope Benchtop SEM at accelerating voltages from 10-15 kV. Compositional differences across each sample were investigated through backscatter electron (BSE) imaging. Energy dispersive X-ray spectroscopy (EDS) provided multielemental, semi-quantitative analysis through point spectra with energy resolution between 130-150 eV. Spectra were collected at 10 kV in BSE mode using a silicon drift detector (SDD). Reacted samples were rinsed twice with Milli-Q (18.2 MΩ cm at 25°C) water before dispersing a small quantity of material on the center of carbon tape adhered to an SEM stub. More than five spot analyses, on six goethite particles were conducted.

Description of the kinetic analysis

We assumed that pseudo-first-order kinetics described systems containing constant $U_{24}Pp_{12}$ concentration and varying mineral concentrations to generate a log-log plot of k'_{rxn} versus *[mineral]* (see Fig. S24). A linear regression of this plot yielded a straight line where b and k_{rxn} were derived from the slope and intercept, respectively, according to equation 1.

$$\log(k'_{rxn}) = \log(-k_{rxn}) + b * \log([mineral]) \qquad (1)$$

Second, we considered a condition with varying $U_{24}Pp_{12}$ concentration and constant mineral concentration to determine k'_{rxn} for each system. A log-log plot of k'_{rxn} versus $[U_{24}Pp_{12}]$ yields a straight line where a and k_{rxn} can be derived from the slope and intercept, respectively, according to equation 2 (see Fig. S25). Because k_{rxn} was negative, the logarithm of $-k_{rxn}$ was not undefined.

$$\log(k'_{rxn}) = \log(-k_{rxn}) + a * \log(U_{24}Pp_{12}) \qquad (2)$$

Since the reaction order with respect to $U_{24}Pp_{12}$ was not one, the initial assumption of first order with respect to $U_{24}Pp_{12}$ was not valid. Therefore, another iteration of the kinetic analysis was performed using the determined values of a and b until the reaction orders converged. This additional iteration utilized the power rule when solving the rate law. Data for this iterative analysis is presented in Figs. S26 – S27.

Similar data for the goethite kinetic analysis is provided in Figs. S28-S31.

Figures

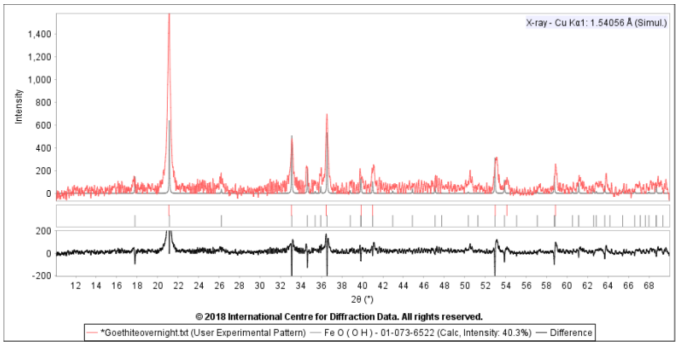

Fig. S1. Powder X-ray diffractogram of 30 mg of goethite (red trace) and PDF 01-073-6522 (black trace).

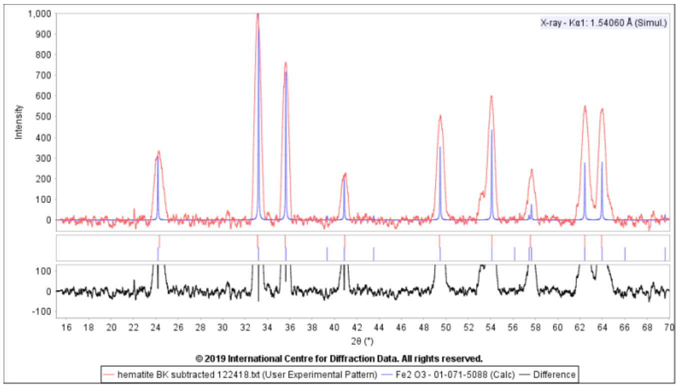

Fig. S2. Powder X-ray diffractogram of 30 mg of hematite (red trace) and PDF 01-071-5088 (blue trace).

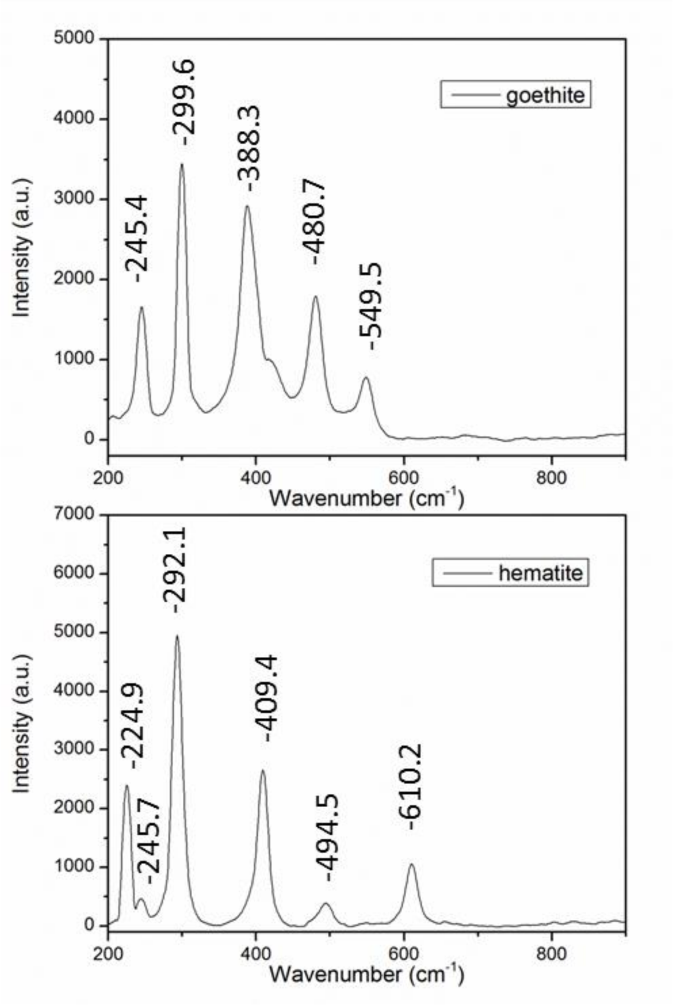

Fig. S3. Raman spectra of goethite (top) and hematite (bottom) with major Raman bands indicated which were matched with published results.[6]

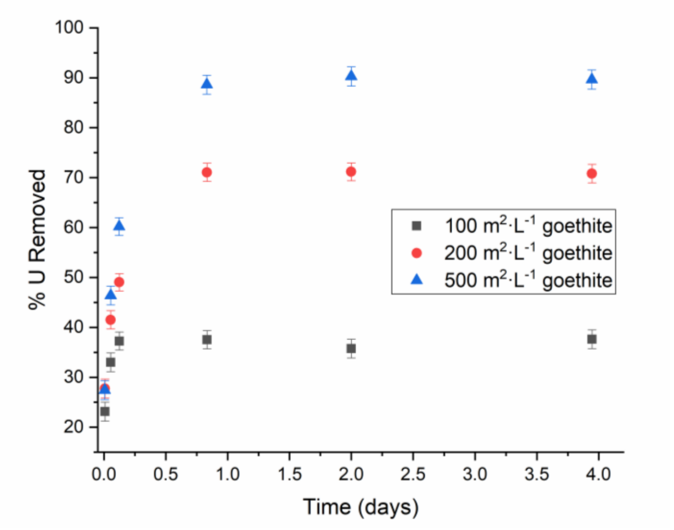

Fig. S4. Removal of uranium from solution as a function of time and goethite concentration in systems containing 0.5 g L^{-1} $U_{24}Pp_{12}$ at pH 9. Data points represent the average of duplicate samples. Error bars represent propagation of error based on the uncertainty of ICP-OES measurements and gravimetric sample preparation.

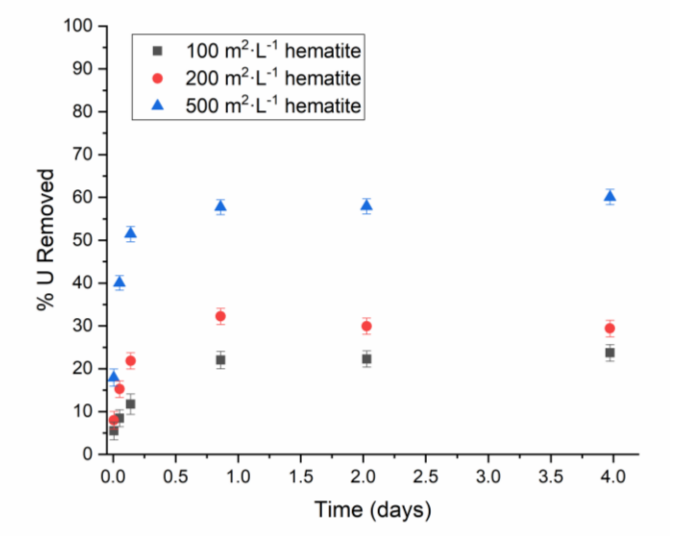

Fig. S5. Removal of uranium from solution as a function of time and hematite concentration in systems containing 0.5 g L^{-1} $U_{24}Pp_{12}$ at pH 9. Data points represent the average of duplicate samples. Error bars represent propagation of error based on the uncertainty of ICP-OES measurements and gravimetric sample preparation.

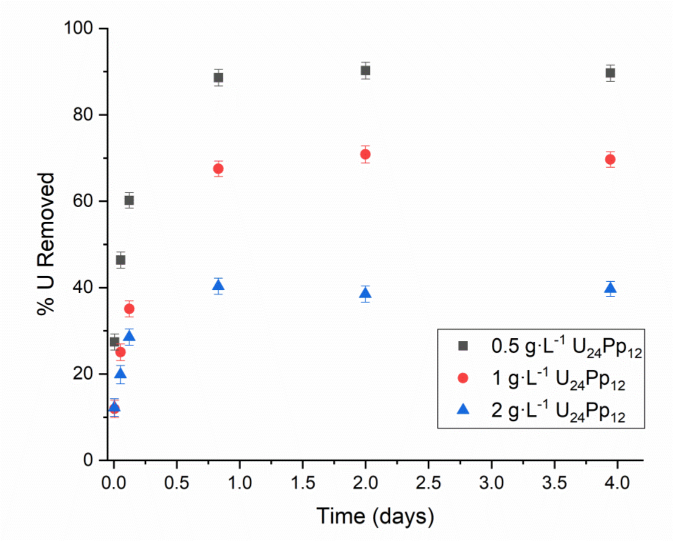

Fig. S6. Removal of uranium from solution as a function of time and $U_{24}Pp_{12}$ concentration in systems containing 500 m^2 L^{-1} goethite at pH 9. Data points represent the average of duplicate samples. Error bars represent propagation of error based on the uncertainty of ICP-OES measurements and gravimetric sample preparation.

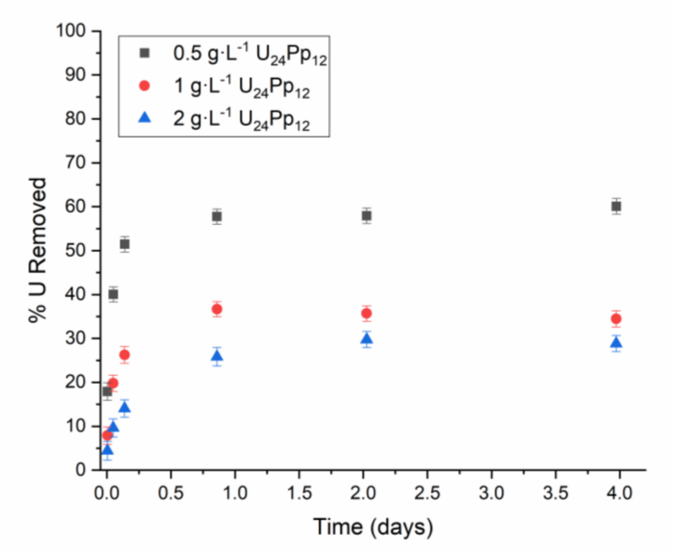

Fig. S7. Removal of uranium from solution as a function of time and $U_{24}Pp_{12}$ concentration in systems containing 500 m^2 L^{-1} hematite at pH 9. Data points represent the average of duplicate samples. Error bars represent propagation of error based on the uncertainty of ICP-OES measurements and gravimetric sample preparation.

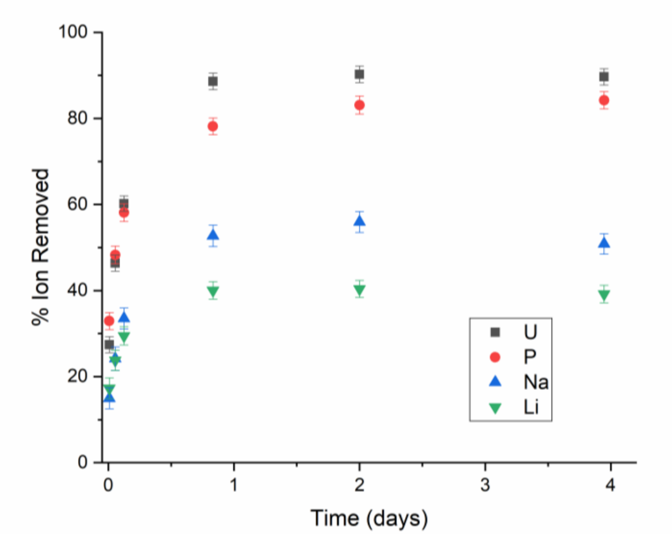

Fig. S8. Percent uranium, phosphorus, sodium, and lithium removed from solution as a function of time in systems containing 0.5 g L^{-1} $U_{24}Pp_{12}$ and 500 m^2 L^{-1} goethite. Values in plots are an average of duplicate experiments. Error bars represent propagation of error based on the uncertainty of ICP-OES measurements.

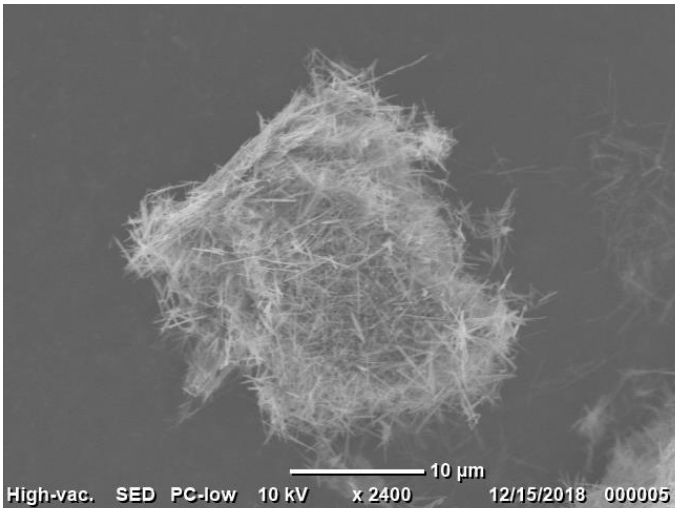

Fig. S9. SEM image of goethite needles.

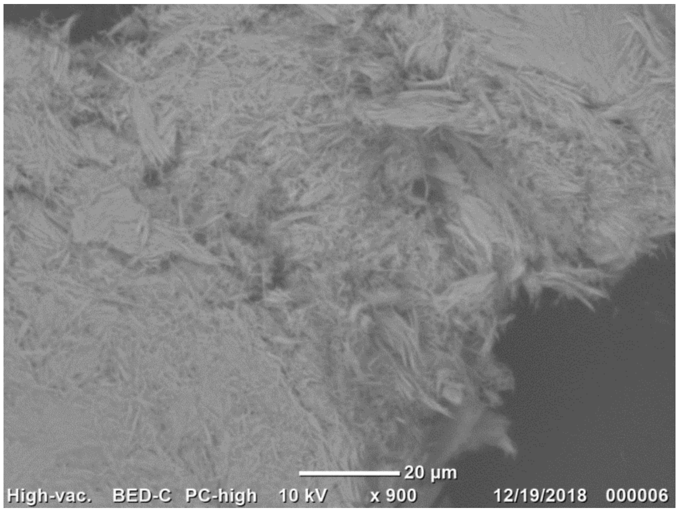

Fig. S10. BSE image of goethite powder reacted with 1 g L^{-1} $U_{24}Pp_{12}$.

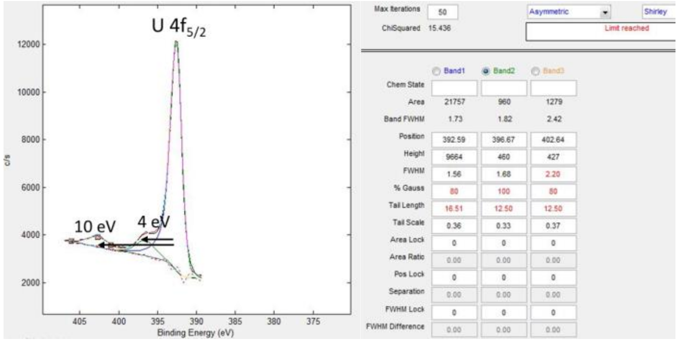

Max Iterations 50
ChiSquared 15.436
Asymmetric
Shirley
Limit reached

	○ Band1	● Band2	○ Band3
Chem State			
Area	21757	960	1279
Band FWHM	1.73	1.82	2.42
Position	392.59	396.67	402.64
Height	9664	460	427
FWHM	1.56	1.68	2.20
% Gauss	80	100	80
Tail Length	16.51	12.50	12.50
Tail Scale	0.36	0.33	0.37
Area Lock	0	0	0
Area Ratio	0.00	0.00	0.00
Pos Lock	0	0	0
Separation	0.00	0.00	0.00
FWHM Lock	0	0	0
FWHM Difference	0.00	0.00	0.00

Fig. S11. U $4f_{5/2}$ binding energy and peak fit parameters of $U_{24}Pp_{12}$ crystals.

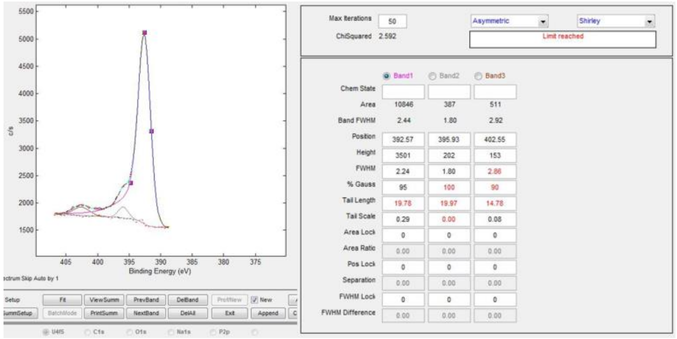

Max Iterations 50
ChiSquared 2.592
Asymmetric
Shirley
Limit reached

	● Band1	○ Band2	○ Band3
Chem State			
Area	10846	387	511
Band FWHM	2.44	1.80	2.92
Position	392.57	395.93	402.55
Height	3501	202	153
FWHM	2.24	1.80	2.86
% Gauss	95	100	90
Tail Length	19.78	19.97	14.78
Tail Scale	0.29	0.00	0.08
Area Lock	0	0	0
Area Ratio	0.00	0.00	0.00
Pos Lock	0	0	0
Separation	0.00	0.00	0.00
FWHM Lock	0	0	0
FWHM Difference	0.00	0.00	0.00

Fig. S12. U $4f_{5/2}$ binding energy and peak fit parameters of 2 g L^{-1} $U_{24}Pp_{12}$ reacted with 500 m^2 L^{-1} goethite.

Max Iterations 50
ChiSquared 4.477
Asymmetric
Shirley
Limit reached

	○ Band1	● Band2	○ Band3
Chem State			
Area	4012	179	290
Band FWHM	2.17	1.85	4.60
Position	392.81	396.46	402.76
Height	1403	87	59
FWHM	1.95	1.81	4.60
% Gauss	80	100	100
Tail Length	18.49	17.28	12.50
Tail Scale	0.33	0.09	0.00
Area Lock	0	0	0
Area Ratio	0.00	0.00	0.00
Pos Lock	0	0	0
Separation	0.00	0.00	0.00
FWHM Lock	0	0	0
FWHM Difference	0.00	0.00	0.00

Fig. S13. U 4*f*$_{5/2}$ binding energy and peak fit parameters of 2 g L^{-1} U$_{24}$Pp$_{12}$ reacted with 500 m^2 L^{-1} hematite.

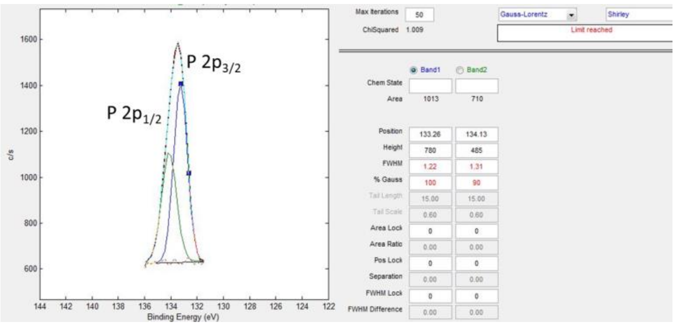

Max Iterations 50
ChiSquared 1.009
Gauss-Lorentz
Shirley
Limit reached

	● Band1	○ Band2
Chem State		
Area	1013	710
Position	133.26	134.13
Height	780	485
FWHM	1.22	1.31
% Gauss	100	90
Tail Length	15.00	15.00
Tail Scale	0.60	0.60
Area Lock	0	0
Area Ratio	0.00	0.00
Pos Lock	0	0
Separation	0.00	0.00
FWHM Lock	0	0
FWHM Difference	0.00	0.00

Fig. S14. P 2*p* binding energy and peak fit parameters of crystals containing U$_{24}$Pp$_{12}$.

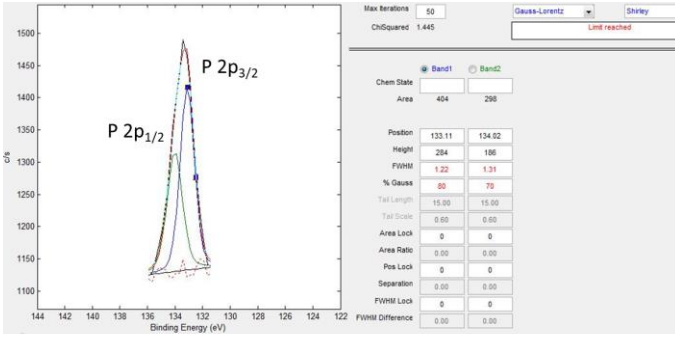

Max Iterations 50
ChiSquared 1.445
Gauss-Lorentz
Shirley
Limit reached

	● Band1	○ Band2
Chem State		
Area	404	298
Position	133.11	134.02
Height	284	186
FWHM	1.22	1.31
% Gauss	80	70
Tail Length	15.00	15.00
Tail Scale	0.60	0.60
Area Lock	0	0
Area Ratio	0.00	0.00
Pos Lock	0	0
Separation	0.00	0.00
FWHM Lock	0	0
FWHM Difference	0.00	0.00

Fig. S15. P 2*p* binding energy and peak fit parameters of the solid phase from a reactor containing 2 mg mL^{-1} U$_{24}$Pp$_{12}$ and 500 m^2 L^{-1} goethite.

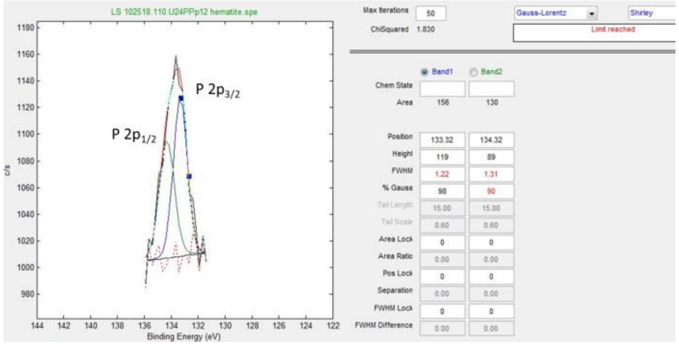

Max Iterations 50

ChiSquared 1.830

Gauss-Lorentz

Shirley

Limit reached

	● Band1	○ Band2
Chem State		
Area	156	130
Position	133.32	134.32
Height	119	89
FWHM	1.22	1.31
% Gauss	98	90
Tail Length	15.00	15.00
Tail Scale	0.60	0.60
Area Lock	0	0
Area Ratio	0.00	0.00
Pos Lock	0	0
Separation	0.00	0.00
FWHM Lock	0	0
FWHM Difference	0.00	0.00

Fig. S16. P 2*p* binding energy and peak fit parameters of the solid phase from a reactor containing 2 mg mL^{-1} $U_{24}Pp_{12}$ and 500 m^{2} L^{-1} hematite.

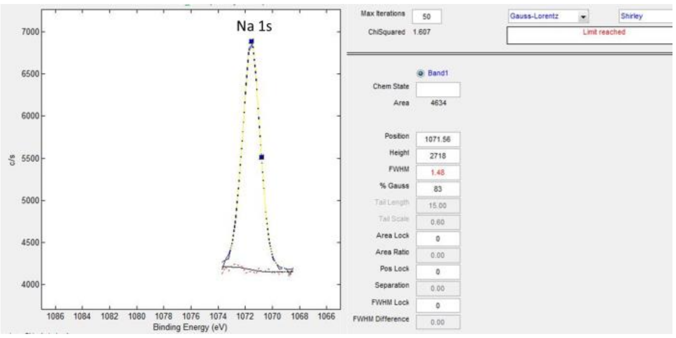

Max Iterations 50

ChiSquared 1.607

Gauss-Lorentz

Shirley

Limit reached

	● Band1
Chem State	
Area	4634
Position	1071.56
Height	2718
FWHM	1.48
% Gauss	83
Tail Length	15.00
Tail Scale	0.60
Area Lock	0
Area Ratio	0.00
Pos Lock	0
Separation	0.00
FWHM Lock	0
FWHM Difference	0.00

Fig. S17. Na 1*s* binding energy and peak fit parameters of crystals containing $U_{24}Pp_{12}$.

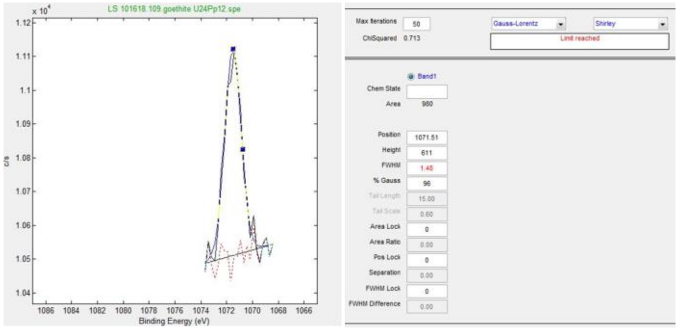

Max Iterations 50

ChiSquared 0.713

Gauss-Lorentz

Shirley

Limit reached

	● Band1
Chem State	
Area	980
Position	1071.51
Height	611
FWHM	1.48
% Gauss	96
Tail Length	15.00
Tail Scale	0.60
Area Lock	0
Area Ratio	0.00
Pos Lock	0
Separation	0.00
FWHM Lock	0
FWHM Difference	0.00

Fig. S18. Na 1*s* binding energy and peak fit parameters of the solid phase from a reactor containing 2 mg mL^{-1} $U_{24}Pp_{12}$ and 500 m^{2} L^{-1} goethite.

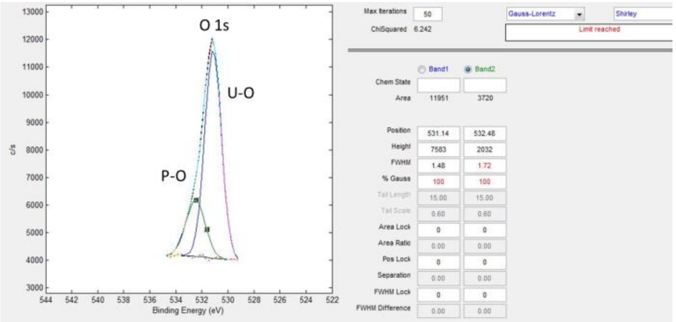

Max Iterations 50
ChiSquared 6.242
Gauss-Lorentz
Shirley
Limit reached

	○ Band1	● Band2
Chem State		
Area	11951	3720
Position	531.14	532.48
Height	7583	2032
FWHM	1.48	1.72
% Gauss	100	100
Tail Length	15.00	15.00
Tail Scale	0.60	0.60
Area Lock	0	0
Area Ratio	0.00	0.00
Pos Lock	0	0
Separation	0.00	0.00
FWHM Lock	0	0
FWHM Difference	0.00	0.00

Fig. S19. O 1*s* binding energy and peak fit parameters of crystals containing $U_{24}Pp_{12}$.

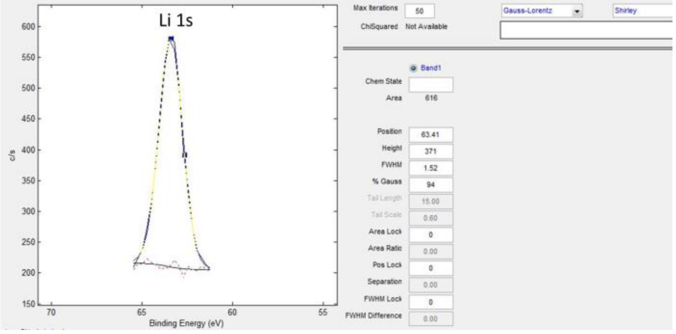

Max Iterations 50
ChiSquared Not Available
Gauss-Lorentz
Shirley

	● Band1
Chem State	
Area	616
Position	63.41
Height	371
FWHM	1.52
% Gauss	94
Tail Length	15.00
Tail Scale	0.60
Area Lock	0
Area Ratio	0.00
Pos Lock	0
Separation	0.00
FWHM Lock	0
FWHM Difference	0.00

Fig. S20. Li 1*s* binding energy and peak fit parameters of crystals containing $U_{24}Pp_{12}$.

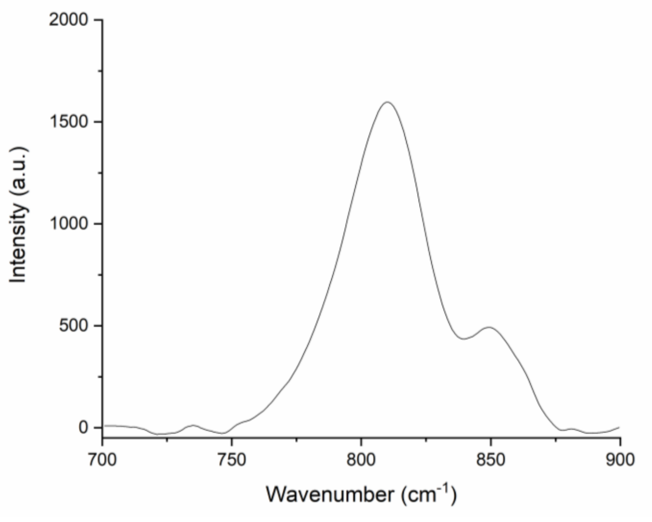

Fig. S21. Raman spectrum of the solid phase from a reaction containing 2 mg mL^{-1} $U_{24}Pp_{12}$ and 500 m^2 L^{-1} goethite. Raman signals at 809.5 cm^{-1} and 853.2 cm^{-1} are assigned to the symmetric stretching of U≡O bonds in the uranyl groups and vibrations of O-O bonds of the bridging peroxo groups, respectively.

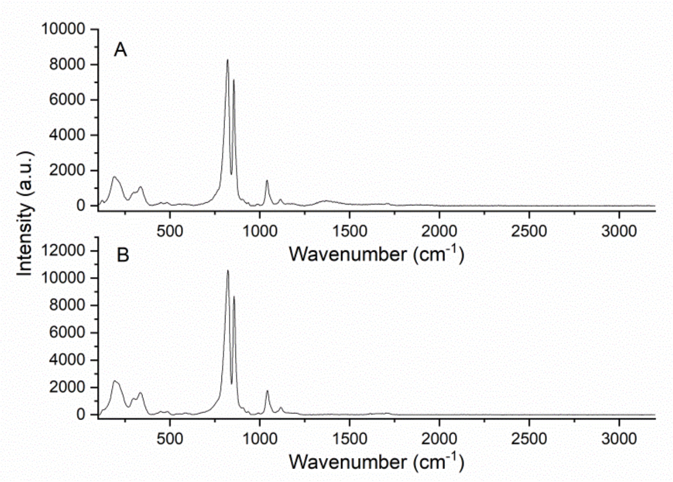

Fig. S22. Raman spectra of powder resulting from solutions containing 2 g L^{-1} $U_{24}Pp_{12}$ at pH 9 that were allowed to air-dry and (A) and crystals containing $U_{24}Pp_{12}$ nanoclusters (B). The main Raman signals at 820 cm^{-1} and 856 cm^{-1} are assigned to the symmetric stretching of U≡O bonds in the uranyl groups and vibrations of O-O bonds of the bridging peroxo groups, respectively.

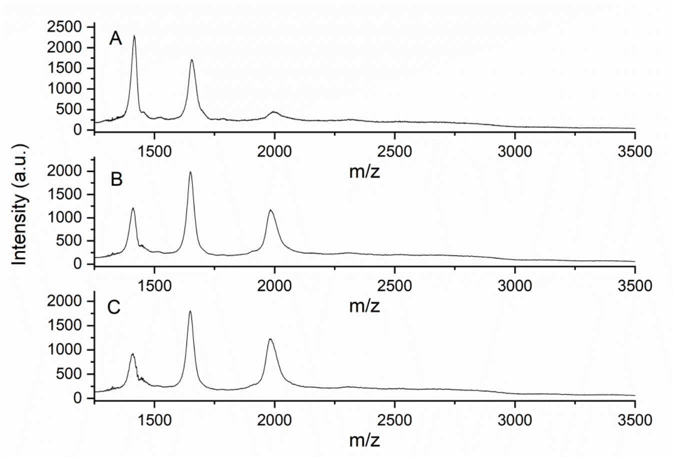

Fig. S23. ESI-MS spectra of 1 g L^{-1} $U_{24}Pp_{12}$ in Milli-Q water (A), 1 g L^{-1} $U_{24}Pp_{12}$ with 500 m^2 L^{-1} goethite (B) and 1 g L^{-1} $U_{24}Pp_{12}$ with 500 m^2 L^{-1} hematite (C) after 4 days.

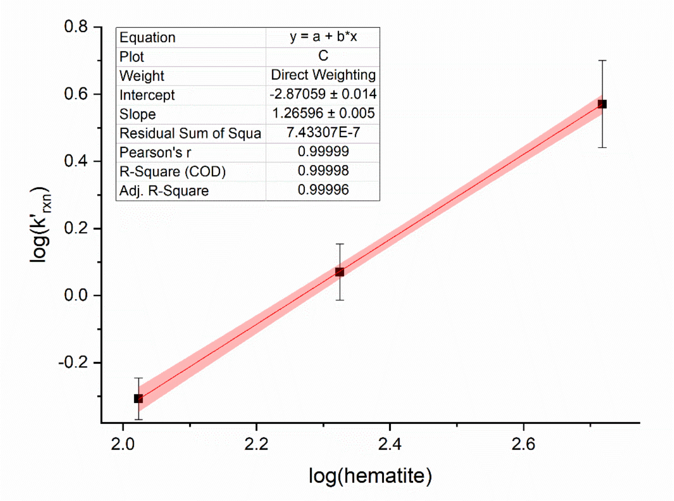

Fig. S24. Dependence of *log(k'$_{rxn}$)* on *log(hematite)* at 0.5 g L^{-1} U$_{24}$Pp$_{12}$. Data points represent the average of duplicate samples. Error bars represent propagation of error based on ICP-OES measurements and gravimetric sample preparation. The red shaded area represents the 95% confidence interval for the linear regression. Raw data is provided in Table S3.

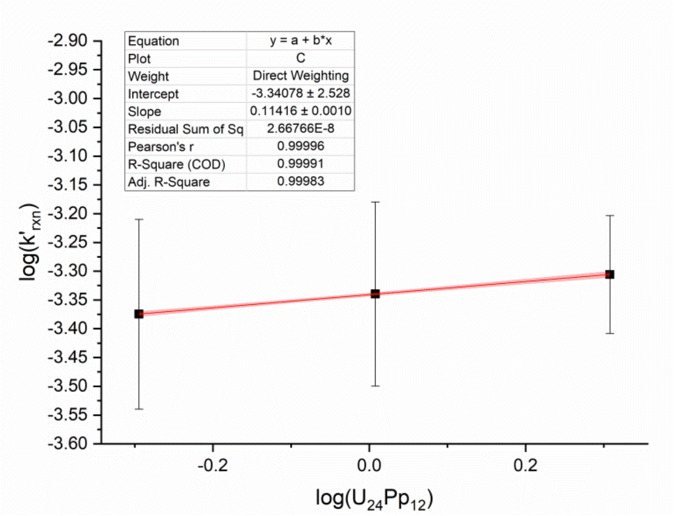

Fig. S25. Dependence of *log(k'$_{rxn}$)* on *log(U$_{24}$Pp$_{12}$)* at 500 m^2 L^{-1} hematite. Data points represent the average of duplicate samples. Error bars represent propagation of error based on ICP-OES measurements and gravimetric sample preparation. The shaded red area represents the 95% confidence interval for the linear regression. Raw data is provided in Table S4.

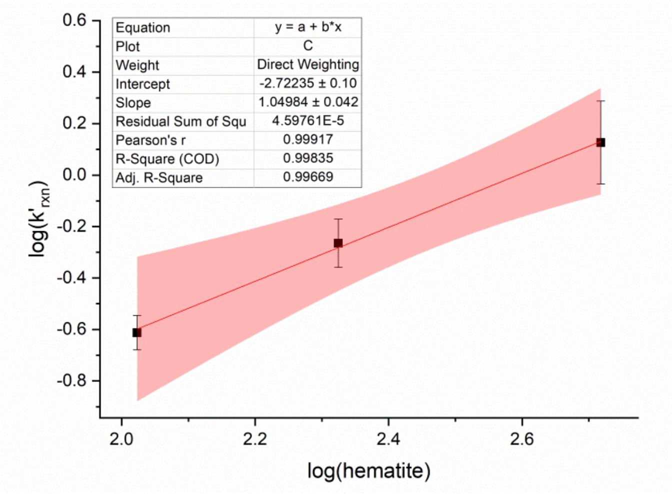

Equation	y = a + b*x
Plot	C
Weight	Direct Weighting
Intercept	-2.72235 ± 0.10
Slope	1.04984 ± 0.042
Residual Sum of Squ	4.59761E-5
Pearson's r	0.99917
R-Square (COD)	0.99835
Adj. R-Square	0.99669

Fig. S26. Dependence of *log(k'*$_{rxn}$*)* on *log(hematite)* at 0.5 g L^{-1} U $U_{24}Pp_{12}$. Data points represent the average of duplicate samples. Error bars represent propagation of error based on ICP-OES measurements and gravimetric sample preparation. The shaded red area represents the 95% confidence interval for the linear regression. Reaction term *b* = 1.05 ± 0.04 and k_{rxn} = (1.9 ± 0.5) x 10^{-3} $(g \cdot L^{-1})^{0.886\pm0.001}$ $(m^2 \cdot L^{-1})^{-1.05\pm0.04}(day^{-1})$.

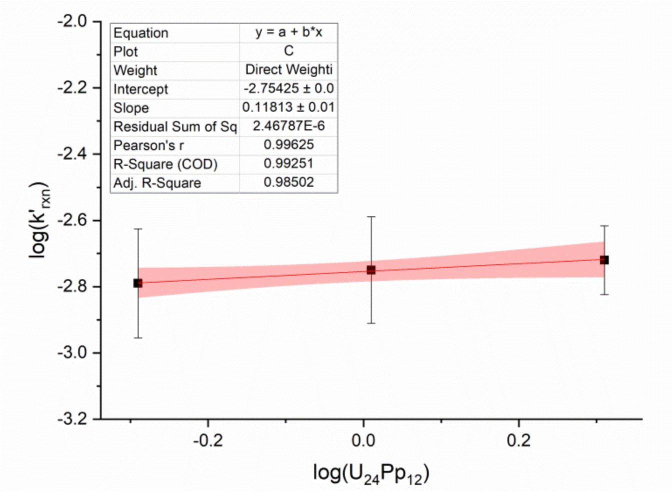

Equation	y = a + b*x
Plot	C
Weight	Direct Weighti
Intercept	-2.75425 ± 0.0
Slope	0.11813 ± 0.01
Residual Sum of Sq	2.46787E-6
Pearson's r	0.99625
R-Square (COD)	0.99251
Adj. R-Square	0.98502

Fig. S27. Dependence of *log(k'*$_{rxn}$*)* on *log(*$U_{24}Pp_{12}$*)* at 500 m^2 L^{-1} hematite. Data points represent the average of duplicate samples. Error bars represent propagation of error based on ICP-OES measurements and gravimetric sample preparation. The red shaded area represents the 95% confidence interval for the linear regression. Reaction term *a* = 0.12 ± 0.01 and k_{rxn} = (1.76 ± 0.01) x 10^{-3} $(g \cdot L^{-1})^{0.88\pm0.01}$ $(m^2 \cdot L^{-1})^{-1.05\pm0.04}$ (day^{-1}).

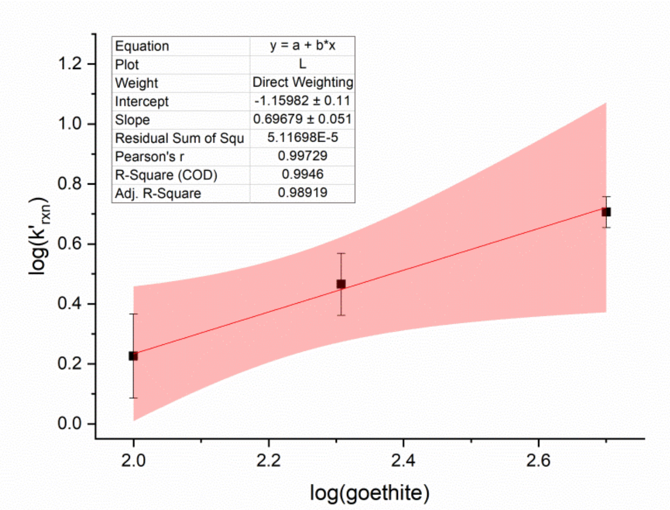

Fig. S28. Dependence of *log*(k'_{rxn}) on *log(goethite)* at 0.5 g L^{-1} $U_{24}Pp_{12}$. Data points represent the average of duplicate samples. Error bars represent propagation of error based on ICP-OES measurements and gravimetric sample preparation. The red shaded area represents the 95% confidence interval for the linear regression. Raw data is provided in Table S5.

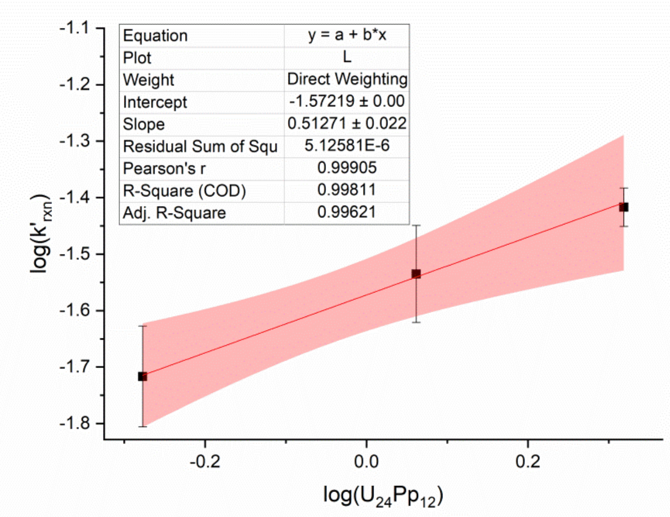

Fig. S29. Dependence of *log*(k'_{rxn}) on *log*($U_{24}Pp_{12}$) in systems containing 500 m^2 L^{-1} goethite. Data points represent the average of duplicate samples. Error bars represent propagation of error based on ICP-OES measurements and gravimetric sample preparation. The red shaded area represents the 95% confidence interval for the linear regression. Raw data is provided in Table S6.

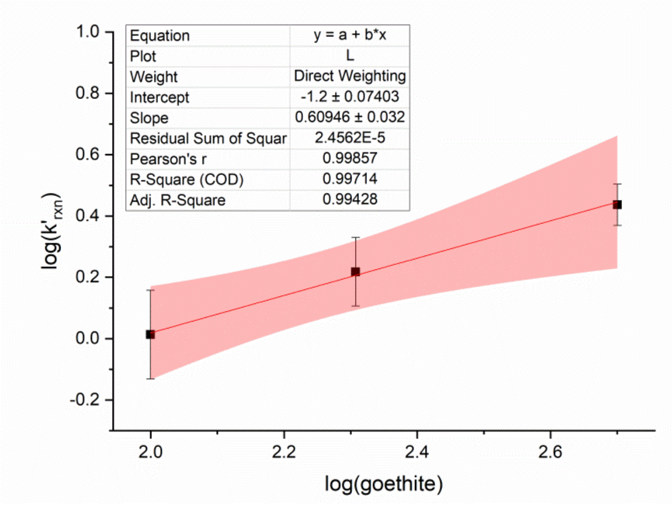

Fig. S30. Dependence of $log(k'_{rxn})$ on *log(goethite)* at 0.5 g L^{-1} U U$_{24}$Pp$_{12}$. Data points represent the average of duplicate samples. Error bars represent propagation of error based on ICP-OES measurements and gravimetric sample preparation. The red shaded area represents the 95% confidence interval for the linear regression. Reaction term *b* = 0.61 ± 0.03 and k$_{rxn}$ = (6 ± 0.1) x 10^{-2} (g·L^{-1})$^{0.49\pm0.02}$ (m^{2}·L^{-1})$^{-0.61\pm0.04}$(day^{-1}).

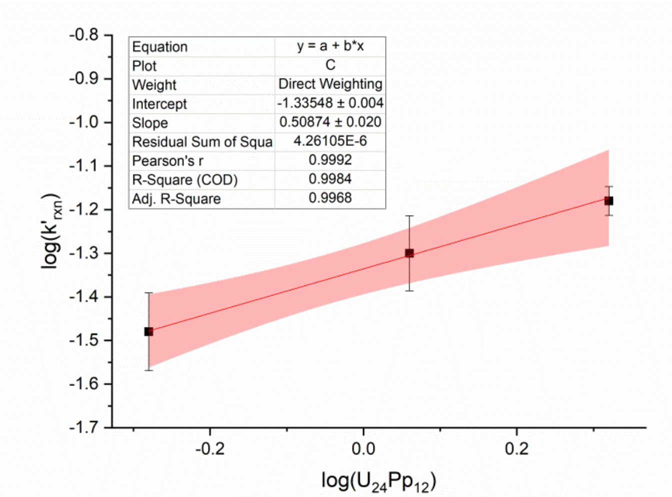

Fig. S31. Dependence of $log(k'_{rxn})$ on $log(U_{24}Pp_{12})$ at 500 m^{2} L^{-1} goethite. Data points represent the average of duplicate samples. Error bars represent propagation of error based on ICP-OES measurements and gravimetric sample preparation. The red shaded area represents the 95% confidence interval for the linear regression. Reaction term *a* = 0.51 ± 0.02 and k$_{rxn}$ = (4.6 ± 0.01) x 10^{-2} (g·L^{-1})$^{0.49\pm0.02}$ (m^{2}·L^{-1})$^{-0.61\pm0.04}$ (day^{-1}).

TABLES

Table S1. Conditions of batch sorption experiments used to determine reaction orders with respect to $U_{24}Pp_{12}$ concentration, *a*, and hematite concentration, *b*.

$U_{24}Pp_{12}$ (g L^{-1})	Hematite (m^2 L^{-1})
0.51 ± 0.01	105 ± 5
0.51 ± 0.01	211 ± 10
0.51 ± 0.01	522 ±25
1.02 ± 0.02	526 ± 25
2.03 ± 0.04	524 ± 25

Table S2. Conditions of batch sorption experiments used to determine reaction orders with respect to $U_{24}Pp_{12}$ concentration, *a*, and goethite concentration, *b*.

$U_{24}Pp_{12}$ (g L^{-1})	Goethite (m^2 L^{-1})
0.52 ± 0.01	100 ± 5
0.51 ± 0.01	203 ± 10
0.53 ± 0.01	501 ±25
1.15 ± 0.02	502 ± 25
2.08 ± 0.03	500 ± 25

Table S3. Raw data supporting the linear regression in Fig. S24.

[Hematite]	Time (days)	$[U\ ppm]_t$	$[U_{24}Pp_{12}\ g\ L^{-1}]_t$
100 m^2 L^{-1}	0.0069	219 ± 4	0.468 ± 0.007
	0.052	212 ± 3	0.453 ± 0.007
	0.141	205 ± 4	0.437 ± 0.009
200 m^2 L^{-1}	0.0062	213 ± 4	0.456 ± 0.007
	0.051	196 ± 3	0.420 ± 0.006
	0.140	181 ± 3	0.387 ± 0.006
500 m^2 L^{-1}	0.0056	191 ± 3	0.408 ± 0.007
	0.051	139 ± 2	0.298 ±0.004
	0.140	113 ± 2	0.241 ± 0.004

Table S4. Raw data supporting the linear regression in Fig. S25.

[$U_{24}Pp_{12}$]	Time (days)	[U ppm]$_t$	[$U_{24}Pp_{12}$ g L^{-1}]$_t$
0.5 g L^{-1}	0.0056	191 ± 3	0.408 ± 0.007
	0.051	139 ± 2	0.298 ± 0.004
	0.140	113 ± 2	0.241 ± 0.004
1 g L^{-1}	0.0049	430 ± 7	0.92 ± 0.01
	0.050	374 ± 5	0.80 ± 0.01
	0.140	344 ± 6	0.74 ± 0.01
2 g L^{-1}	0.0042	889 ± 15	1.90 ± 0.03
	0.049	841 ± 14	1.80 ± 0.03
	0.138	800 ± 13	1.71 ± 0.03

Table S5. Raw data supporting the linear regressions in Fig. S28.

[Goethite]	Time (days)	[U ppm]$_t$	[$U_{24}Pp_{12}$ g L^{-1}]$_t$
100 m^2 L^{-1}	0.0083	189 ± 3	0.403 ± 0.006
	0.056	164 ± 3	0.351 ± 0.006
	0.125	154 ± 2	0.329 ± 0.005
200 m^2 L^{-1}	0.0076	173 ± 3	0.369 ± 0.006
	0.055	140 ± 2	0.300 ± 0.005
	0.124	122 ± 2	0.261 ± 0.004
500 m^2 L^{-1}	0.0069	179 ± 3	0.383 ± 0.006
	0.054	133 ± 2	0.283 ± 0.005
	0.124	98 ± 2	0.210 ± 0.003

Table S6. Raw data supporting the linear regression in Fig. S29.

[$U_{24}Pp_{12}$]	Time (days)	[U ppm]$_t$	[$U_{24}Pp_{12}$ g L^{-1}]$_t$
0.5 g L^{-1}	0.0069	179 ± 3	0.383 ± 0.006
	0.054	133 ± 2	0.283 ± 0.005
	0.124	98 ± 2	0.210 ± 0.003
1 g L^{-1}	0.0062	478 ± 8	1.02 ± 0.02
	0.054	407 ± 7	0.87 ± 0.02
	0.123	354 ± 6	0.76 ± 0.01
2 g L^{-1}	0.0056	856 ± 14	1.83 ± 0.03
	0.053	781 ± 15	1.67 ± 0.03
	0.122	697 ± 11	1.49 ± 0.02

References

1 B.T. McGrail, G.E. Sigmon, L.J. Jouffret, C.R. Andrews, P.C. Burns, Raman Spectroscopic and ESI-MS Characterization of Uranyl Peroxide Cage Clusters, *Inorg. Chem.* 2014, **53**, 1562-1569.

2 D.A. Shirley, High-Resolution X-Ray Photoemission Spectrum of the Valence Bands of Gold, *Phys. Rev. B* 1972, **5**, 4709–4714.

3 M. Schindler, F.C. Hawthorne, M.S. Freund, P.C. Burns, XPS spectra of uranyl minerals and synthetic uranyl compounds. I: The U4f spectrum, *Geochim. Cosmochim. Acta* 2009, **73**, 2471-2487.

4 T.-C. Lin, G. Seshadri, J.A. Kelber, A consistent method for quantitative XPS peak analysis of thin oxide films on clean polycrystalline iron surfaces, *Appl. Surf. Sci.* 1997, **119**, 83-92.

5 J.F. Moulder, W.F. Stickle, P.E. Sobol, K.D. Bomben, *Handbook of X-ray Photoelectron Spectroscopy: A Reference Book of Standard Spectra for Identification and Interpretation of XPS Data*, ed. J. Chastain, Perkin-Elmer Corporation, Eden Prairie, MN, 1992.

6 M. Hanesch, Raman spectroscopy of iron oxides and (oxy)hydroxides at low laser power and possible applications in environmental magnetic studies, *Geophys. J. Int.* 2009, **177**, 941-948.